Available online at www.sciencedirect.com
ScienceDirect
Journal of Power Sources 163 (2007) 755–767
JOURNAL OF POWER SOURCES
www.elsevier.com/locate/jpowsour

Review

Metal bipolar plates for PEM fuel cell—A review

H. Tawfik [a,*], Y. Hung [a,c], D. Mahajan [b,c]

[a] *Institute for Research and Tech. Transfer, Farmingdale State University of New York, Farmingdale, NY, USA*
[b] *Energy Sciences & Technology Department, Brookhaven National Laboratory, NY 11973-5000, USA*
[c] *Chemical and Molecular Engineering Program, Stony Brook University, Stony Brook, NY 11794, USA*

Received 21 August 2006; received in revised form 26 September 2006; accepted 27 September 2006
Available online 20 November 2006

Abstract

The polymer electrolyte membrane (PEM) based fuel cells are clean alternative energy systems that hold excellent potential for cost effectiveness, durability, and relatively high overall efficiency. PEM fuel cell is recognized by the U.S. Department of Energy (DOE) as the main candidate to replace the internal combustion engine in transportation applications. Metallic bipolar plates and membrane electrode assembly (MEA) are two crucial components of a PEM power stack and their durability and fabrication cost must be optimized to allow fuel cells to penetrate the commercial market and compete with other energy sources.

The bipolar plates perform as the current conductors between cells, provide conduits for reactant gases flow, and constitute the backbone of a power stack. They are commonly made of graphite composite for high corrosion resistance and good surface contact resistance; however their manufacturability, permeability, and durability for shock and vibration are unfavorable in comparison to metals. On the other hand, various methods and techniques must be developed to combat metallic corrosion and eliminate the passive layer that causes unacceptable reduction in contact resistance and possible fouling of the catalyst and the ionomer. Thus recently metallic bipolar plates have received considerable attention in the research community. This paper offers a comprehensive review of the research work conducted on metal bipolar plates to prevent corrosion while maintaining a low contact resistance.

Keywords: Hydrogen fuel cell; Bipolar plate; Review

Contents

* Corresponding author. Tel.: +1 631 420 2307; fax: +1 631 420 2194.
E-mail address: TAWFIKHH@FARMINGDALE.EDU (H. Tawfik).

0378-7753/$ – see front matter © 2006 Elsevier B.V. All rights reserved.
doi:10.1016/j.jpowsour.2006.09.088

1. Introduction

Bipolar plates constitute the backbone of a hydrogen fuel cell power stack, conduct current between cells, facilitate water and thermal management through the cell, and provide conduits for reactant gases namely hydrogen and oxygen. In the polymer electrolyte membrane (PEM) hydrogen fuel cell design, bipolar plates are fabricated in mass production and they must be made of materials with excellent manufacturability and suitable for cost-effective high volume automated production systems. Currently, graphite composites are considered the standard material for PEM bipolar plates because of its low surface contact resistance and high corrosion resistance. Unfortunately, graphite and graphite composites are classified as brittle and permeable to gases with poor cost effectiveness for high volume manufacturing processes relative to metals such as aluminum, stainless steel, nickel, titanium, etc. Since durability and cost represent the two main challenges hindering the fuel technology from penetrating the energy market and competing with other energy systems, considerable attention was recently given to metallic bipolar plates for their particular suitability to transportation applications. Metals enjoy higher mechanical strength, better durability to shocks and vibration, no permeability, and much superior manufacturability and cost effectiveness when compared to carbon-based materials, namely carbon–carbon and carbon–polymer composites. However, the main handicap of metals is the lack of ability to combat corrosion in the harsh acidic and humid environment inside the PEM fuel cell without forming oxidants, passive layers, and metal ions that cause considerable power degradation. Considerable attempts are being made using noble metals, stainless steel and various coated materials with nitride- and carbide-based alloys to improve the corrosion resistance of the metals used without sacrificing surface contact resistance and maintaining cost effectiveness. Gold-coated titanium and niobium were the materials used by General Electric in the 1960s [1] that were later replaced by graphite composites to reduce cost and weight. In recent years, due to lack of graphite durability under mechanical shocks and vibration combined with cost effectiveness concerns of its high volume manufacturability, considerable research work is currently underway to develop metallic bipolar plates with high corrosion resistance, low surface contact resistance, and inexpensive mass production.

Various types of metals and alloys are currently under testing and evaluation by researchers working in the field of PEM fuel cells to develop bipolar plates that posses the combined merits of graphite and metals. The ideal characteristics of a bipolar plate's material is high corrosion resistance and low surface contact resistance, like graphite, and high mechanical strength, no permeability to reactant gases and no brittleness like metals such as stainless steel, aluminum, titanium, etc. The main challenge however is that corrosion-resistant metal bipolar plates develop a passivating oxide layer on the surface that does protect the bulk metal from progression of corrosion, but also cause an undesirable effect of a high surface contact resistance. This causes the dissipation of some electric energy into heat and a reduction in the overall efficiency of the fuel cell power stack. The key characteristics of bipolar plates material that are suitable for transportation applications are as follows:

- high corrosion resistance with corrosion current at 0.1 V and H_2 purge $< 16\,\mu A\,cm^{-2}$;
- high corrosion resistance with corrosion current at 0.6 V and air purge $< 16\,\mu A\,cm^{-2}$;
- interfacial contact resistance (ICR) @$140\,N\,cm^{-2} = 20\,m\Omega\,cm^2$;
- does not dissolve and produce metal ions;
- possess steady low Ohmic resistance throughout the operation;
- high surface tension with water contact angle close to 90 °C, i.e. high dehydration;
- light weight;
- high mechanical strength $< 200\,N\,m^{-2}$;
- high volume cost-effective manufacturability: US$ $10\,kW^{-1}$.

2. Background and review

Poco graphite has been considered as the PEM fuel cell industry standard for bipolar plates because of its excellent corrosion resistance, interfacial contact resistance, surface energy, and contact angle. However, its brittleness and lack of mechanical strength combined with its relatively poor cost effectiveness for large volume manufacturing, Poco graphite bipolar plate is deemed unsuitable for automotive application and commercialization. Accordingly, a number of materials are currently being developed and tested in laboratories around the world to produce cost-effective and durable bipolar plates for polymer electrolyte membrane fuel cell (PEM). Varieties of non-coated and coated metals, metal foams and non-metal graphite composites are being reviewed for possible replacement of Poco graphite. Below we describe each of these approaches and their state of advancement for potential application in fuel cells.

2.1. Precious non-coated metals

Nobel metals such as gold and platinum perform very similar to Poco graphite bipolar plates [2] and in some cases showed more superior performance. However, the high cost of these metals has prohibited their utilization for commercial use.

2.2. Non-coated metals

Major concerns have been the extent of corrosion (and its products) and a decrease in contact resistance values once surface passivation film forms. Candidates such as stainless steel have been tested and used as bipolar plates (BPs) by different authors. Hermann et al. [3] reported that aluminum, stainless steel, titanium, and nickel (BP) exposed to an operating environment similar to that of a fuel cell with a pH of 2–3 at temperatures around 80 °C are prone to corrosion or dissolution. Moreover, a corrosion layer on the surface of a BP increases electrical resistance and decreases output of the cell. While this surface oxide layer protect the metal and stops the corrosion from progressing further through the lower layers (beneath the surface), it forms however an electrically insulating interfacial layer. As the thickness of the oxide layer increases the electrical surface contact resistance also increases that accordingly cause a decrease in the electric power.

Davies et al. [4] indicated that the relative interfacial resistance of various grades of stainless steel decreased in the order 321 > 304 > 347 > 316 > Ti > 310 > 904 > Incoloy 800 > Inconel 601 > Poco graphite, under compaction 'force' imposed for the fuel cell experiments of the values at 220 N cm^{-2}. For high alloy materials, the authors observed that the oxygen was not as prominent as that illustrated for other grades of stainless steel, which suggests that the passive film was thinner in these samples. The results showed that the passive film decreased in thickness according to the order 321 > 304 > 316 > 347 > 310 > 904 > Incoloy 800 > Inconel 601. Poco graphite, with the lowest surface resistive losses, produced the highest potentials, with increased polarization observed for metal plates in the order Poco graphite < 310 < Ti < 316. This clearly indicates that the performance of the bipolar plate is significantly related to the thickness of passive layer and surface contact resistance: as the thickness and contact resistance increase, more heat energy is generated and less output electric energy is produced.

Wang et al. [5,6] found that both austenitic (349TM) and ferritic (AISI446) stainless steel with high Cr content showed good corrosion resistance and could be suitable for bipolar plates though AISI446 requires some improvement in contact resistance due to formation of a surface passive layer of Cr_2O_3. They also verified that Cr in the alloy forms passive film on the surface of stainless steel. As the Cr content in stainless steel increased, the corrosion-resistance improved that agreed with the findings of Davies et al. [4]. However, a thick non-conductive surface passive layer of Cr_2O_3 will produce an undesirable low surface contact resistance. Wang and Turner [6] studied stainless steel samples of AISI434, AISI436, AISI441, AISI444, and AISI446. They noted that in both PEM fuel cell anode and cathode environments, AISI446 steel underwent passivation and the formed passive films were very stable. An increase in ICR between the steel and the carbon backing material due to passive film formation was also reported. The same authors indicated that the thickness of passive film on AISI446 was estimated to be 2.6 nm for the film formed at 0.1 V in the simulated PEM fuel cell anodic environment and 3.0 nm for the film formed at 0.6 V in the simulated PEM fuel cell cathodic environment. The authors recommended that further improvement in the ICR will require some modification of the passive film, which is dominated by chromium oxide. They also stated that ICR for AISI446 increased after passivation. XPS depth profiles indicated that air-formed surface film was composed of iron oxides and chromium oxide but neither dominated. The passive films on AISI446 were mainly chromium oxide, and the iron oxides played only a minor role. In simulations of the PEMFC, the passive film formed on the cathode was thicker than that formed on the anode, with the former resulting in higher ICR.

The surface oxide layer of metals such as Al, Ti, Ni, etc. similarly forms a surface passive layer that has good corrosion resistance but poor surface contact resistance. Moreover, uncoated metal ions and oxides could directly foul the electrolyte and tarnish the catalyst in the MEA that results in considerable adverse effects on the cell performance. Specifically, as non-protected metal bipolar plates are exposed to the harsh operating environment inside the fuel cell which is very conducive to corrosion with relative humidity of more than 90%, high acidity (pH 2–3) and temperature range of 60–80 °C, metal dissolution will occur. The dissolved metal ions diffuse into the membrane and then get trapped in the ion exchange sites inside the ionomer, resulting in lowered ionic conductivity as described by Mehta and Cooper [7]. A highly conductive corrosion resistance coating with high bonding strength at the interfacial layer between base metal substrate and coating layer is required to minimize this problem.

2.3. Coated metals

Metallic bipolar plates are coated with protective coating layers to avoid corrosion. Coatings should be conductive and adhere to the base metal without exposing the substrate to corrosive media [8]. Two types of coatings, carbon-based and metal-based, have been investigated [7–9]. Carbon-based coatings include graphite, conductive polymer, diamond-like carbon, and organic self-assembled monopolymers [3]. Noble metals, metal nitrides and metal carbides are some of the metal-based coatings. Further, the coefficient of thermal expansion of base metal and the coating should be as close as possible to eliminate formation of micro pores and micro cracks in coatings due to unequal expansion [9]. In addition, some coating processes are prone to pinhole defects and viable techniques for coating bipolar plates are still under development [3]. Mehta and Cooper [7] presented an overview of carbon-based and metallic bipolar plate coating materials. Carbon-based coatings include: (1) graphite, (2) conductive polymer, (3) diamond like carbon, (4) organic self-assembled monopolymers. Metal-based coatings include: (5) noble metals, (6) metal nitrides, (7) metal carbides. Table 1 lists bipolar plate coatings and coating techniques summarized by several groups to date.

Woodman et al. [9] concluded that the coefficient of thermal expansion (CTE), corrosion resistance of coating, and micro pores and micro cracks play a vital role in protecting bipolar plates from the hostile PEM fuel cell environment. The authors also argue that even though PEM fuel cells typically

Table 1
Coating materials and coating processes for metallic bipolar plates [3,7]

Coating method	Coating materials	Coating processes	Base plate materials				Ref.
			Al	SS	Ti	Ni	
Conductive polymers coating	Conductive polymers	Not specified	Not specified				[8]
Diamond-like carbon coating	Diamond-like carbon	Not specified	Not specified				[8]
Gold topcoat layering	Gold over nickel over copper	Pulse current electrodeposition	×				[9,11]
Graphite foil layering	(1) Sublayer—sonicated graphite particles in an emulsion, suspension or paint (e.g. graphite particles in an epoxy resin thinned by an organic solvent, such as toluene); (2) topcoat—exfoliated graphite in the form of sheets of flexible, graphite foil	Painting OR pressing	×		×	×	[45]
Graphite topcoat layering	(1) Sublayer—titanium over titanium–aluminum-nitride; (2a) overcoat—transient metal sublayer of Cr (Ti, Ni, Fe, Co) followed by sulfuric/chromic acid OR; (2b) topcoat—graphite	PVD (closed-field, unbalanced, magnetron sputter ion plating) and chemical anodization/oxidation overcoating	×	×	×	×	[45]
Indium doped tin oxide layering	Indium doped tin oxide ($Sn(In)O_2$)	Electron beam evaporation		×			[46]
Lead oxide layering	(1) Sublayer—lead; (2) topcoat—lead oxide (PbO/PbO_2)	Vapor deposition and sputtering		×			[46]
Organic monopolymer coating	Organic self-assembled monopolymers	Not specified	Not specified				[8]
Silicon carbide layering	(1) n-Type silicon carbide (SiC); (2) gold	Glow discharge decomposition and vapor deposition		×			[46]
Stainless steel layering	(1) Sublayer— chromium/nickel/molybdenum-rich stainless steel OR nickel–phosphorus alloy; (2) topcoat—titanium-nitride	Physical vapor deposition (PVD) (e.g. magnetron sputtering), or chemical vapor deposition (CVD), and electroless deposition for Ni–Ph alloy	×	×	×		[47]
Titanium–aluminum-nitride layering	Titanium–aluminum-nitride layer	RF-planar magnetron (sputtering)	×				[46]
Titanium-nitride layering	Titanium-nitride (TiN) layer	RF-diode sputtering			×		[46]

operate at temperatures less than 100 °C, vehicle service would impose frequent start up and shut down conditions, and temperature differentials of 75–125 °C would be expected during typical driving conditions. A large difference in the CTE of the substrate and coating materials may lead to coating layer failure. One technique to minimize the CTE differential is to add intermediate coating layers with CTEs between that of adjacent layers. Materials such as Al, Cu, and Ni, are very susceptible to electrochemical corrosion in acidic solutions that are typical of PEMFC operating conditions. However, materials such as Au and phosphorous Ni show very high resistance to electrochemical corrosion, comparable to graphite, the traditional bipolar plate material.

2.3.1. Metal-based coatings

2.3.1.1. Gold-plated Al. Hentall et al. [10] machined current collectors from Al to the exact dimensions of graphite bipolar plates, then coated with Au by a solution process. The plates were then used in a fuel cell and during the initial warm-up procedure; the data indicated performance very similar to graphite 1.2 A cm^{-2} at 0.5 V. However, very quickly the performance degraded to 60 mA cm^{-2} at 0.5 V. The analysis revealed that some of the Au layer lifted from the plate and became embedded in the membrane. Wind et al. [2] also indicated that Au-coated bipolar plate (316SS) clearly demonstrated no difference between the metal-based and graphite plates.

Woodman et al. [9] measured the coefficient of thermal expansion (CTE) for aluminum to be approximately 24 μin. $in.^{-1}$ $°C^{-1}$ (over 0–400 °C) while the CTE for Au, for example, was approximately 14 μin. $in.^{-1}$ $°C^{-1}$ over the same temperature range. The authors concluded that the differential of thermal expansion was 0.11% at 120 °C and the mechanism for coating failure was an initiation of plastic deformation of the coating material. The failure of Au coating would be expected at a differential expansion of only 0.08% once the plastic deformed.

Due to high price of Au-coated bipolar plates, this technology stands to face extreme competition from other less expensive corrosion-resistant coatings for bipolar plates (Table 2). Also, coating techniques and surface preparation must be optimized to improve the bonding strength between Au coating and the substrate base plate to eliminate the possibility of separation. The graphite bipolar plate has a material cost of US$ 89 kW^{-1} whereas the Au-coated Al has a cost of US$ 346 kW^{-1}. Using a non-coated Al bipolar plate gives a material cost of US$ 2.71 kW^{-1}. For example, using a nickel coating on Al gives a bipolar plate cost of US$ 3.20 kW^{-1} [11].

Table 2
Bipolar plate materials and high-volume material costs

Material	Material cost (US$ g^{-1})	Density (g cm^{-3})
Graphite	0.105	1.79
Aluminum	0.0088	2.7
Gold	9.97	19.32
Electroless nickel	0.034	8.19

2.3.1.2. TiN-coated bipolar plates. Li et al. [12] investigated the corrosion behavior of TiN-coated type 316 stainless steel in a simulated PEMFC environment, i.e. 0.01 M HCl/0.01 M Na_2SO_4 solutions bubbled with pure O_2 and H_2 gases, respectively, by using electrochemical measurement techniques. They observed that TiN coatings had much better corrosion resistance and passivity under both simulated conditions than stainless steel with no significant degradation of TiN coatings took place in 4 h under typical load conditions of a fuel cell. The authors reported a loss of small part of coatings that had occurred during the immersion tests of TiN coatings in the O_2 environment for 1000 h and in the H_2 environment for 240 h, respectively, but the exposed substrate areas were passivated in both environments. The results revealed that TiN coating can offer 316SS higher corrosion resistance and electric conductivity than 316SS. Further effort to improve the coating quality and evaluation of the long-term stability of 316SS/TiN coating system under simulated conditions are required.

Similar work was conducted by Cho et al. [13]. They observed significant improvement in the lifetime of 316SS stainless steel bipolar plates coated with corrosion-protective TiN layer. The coating process began with chemical etching of 1.5 mm thick 316SS stainless steel bipolar plates to form flow channels. This was followed by coating the surface of the plates with TiN layer using hollow cathode discharge (HCD) ion plating method The HCD system consisted of a vacuum chamber with a pressure of 3×10^{-6} Torr which was then purged with Ar gas in which the etched plates were placed and a Ti target was evaporated at a discharge voltage of 260 V. N_2 gas with an operating pressure of 6.3×10^{-3} Torr was fed at a flow rate of 160 standard cubic centimeter (sccm) to form 1 μm thick TiN layer on the surface of the plates.

Surface energy and surface contact resistance of bipolar plates are other important factors affecting cell performance particularly at high current densities since water produced by the cathode reaction should be immediately removed to avoid flooding and power degradation due to catalyst submergence. High contact resistance of the bipolar plates will also reduce electric energy output due to partial conversion to heat energy. Bipolar plates with low surface energy, low water contact angle (>90° and high) surface wetability could directly contribute to flooding of cathode side of the fuel cell. To evaluate surface energy of different materials, the water contact angle could be measured and evaluated. High contact angle is an indication of a high surface energy or surface tension of a material and low surface wetability. For instance, water contact angle of graphite and TiN-coated 316 was almost same and equal to 90° while that of 316 stainless steel was 60°. The results obtained by Cho et al. [13] imply that 316 stainless steel has low surface energy and more readily floods the cathode side than graphite and TiN-coated 316SS. The authors also stated that the dissolution of metallic elements such as Fe, Ni, Cr, and Ti from TiN-coated 316 bipolar plates into the MEA could increase Ohmic resistance and charge transfer resistance of the single cell by contaminating the membrane and active catalytic sites.

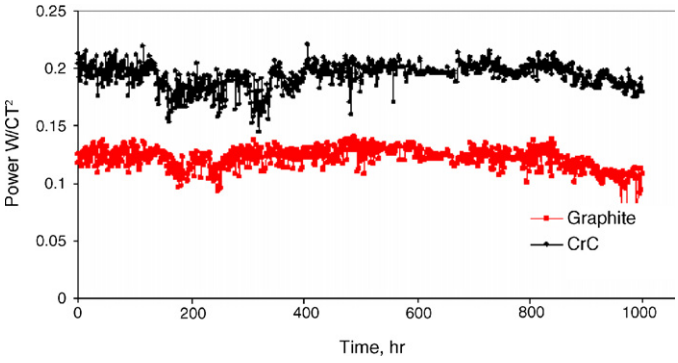

Fig. 1. Single cell (6.45 cm^2 active area) lifetime testing of graphite composite and carbide-based coated aluminum plates at 70 °C Tawfik and co-workers [16].

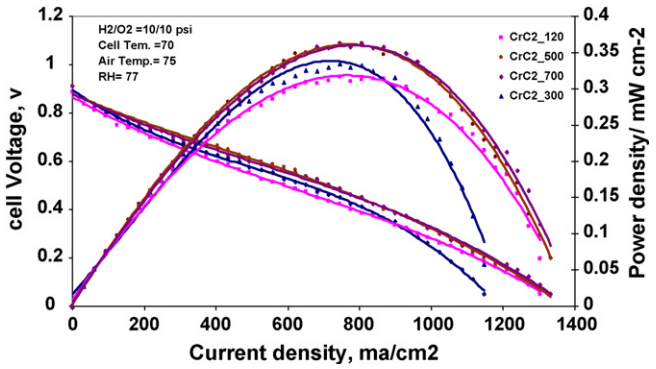

Fig. 2. Polarization and power curves through 1000 h of operation for carbide-based coating at various operation hours; maximum percentage difference: −0.33.

2.3.1.3. CrN/Cr_2N coating on a model Ni–Cr alloy. Brady et al. [14] have recently developed a preferential thermal nitridation process to form defect-free coatings or a pinhole free CrN/Cr_2N coating on a Ni–Cr alloy base plate, which show promise with excellent corrosion resistance and negligible contact resistance. They pointed out that dense, electrically conductive, corrosion-resistant Cr-nitride surfaces can be formed on Ni–Cr and Ni(Fe)–Cr base alloys at Cr levels < 35 weight percent by thermal nitridation. They added that nitridation of 446 stainless steel (and likely other Fe–Cr base alloys), under certain conditions that modify the native passive oxide layer but do not form a dense Cr-nitride surface, can lower ICR by over an order of magnitude without compromising corrosion resistance. Both of these surface modifications show promise for protecting metallic bipolar plates in PEMFC environments.

2.3.1.4. Carbide-based amorphous metallic coating alloy. Tawfik and co-workers [15,16] developed a high corrosion-resistant coating which was fabricated of a full densification carbide-based amorphous alloy and applied to both aluminum and stainless steel bipolar plates. A single cell with 6.25 cm^2 active area performed superior to an identical graphite composite cell operated under the same conditions and the input parameters. Fig. 1 depicts the output performance and real-time testing of both cells, namely graphite composite and metallic bipolar plates conducted under cyclic loading at 70 °C for 1000 h with essentially no power degradation. The high bonding strength between the coating and the substrate combined with comparable coefficient of thermal expansion (CTE) for both metals have precluded the possibility of coating delamination. The full coating densification nature produced by the high velocity oxygen fuel (HVOF) thermal spray system minimized the existence of nano/micro cracks or pinholes in the coating layer that could jeopardize its full proof corrosion protection and complete prevention of corrosive mediums from reaching the substrate. Further studies to examine the coating durability and integrity are recommended.

The carbide-based coating applied on the aluminum bipolar plates for corrosion protection showed excellent durability for harsh corrosive environment inside the fuel cell. Fig. 2 displays the small variation in both power density and polarization curves during the 1000 h of operation using the single cell carbide-based coating bipolar plates. The consistency of the performance is a clear indication of the following: (1) lack of formation of oxide or passive layer that is usually associated with increase in the surface contact resistance and drop in electric power output; (2) lack of metal ion poisoning of the ionomer due to metal dissolution; (3) no tarnishing of the catalyst.

The electrochemical testing of the alloy showed the corrosion current to be within an order of magnitude of that for the graphite composite. Fig. 3 exhibits the corrosion rate of various metals and coatings measured by Tafel electrochemical potentiodynamic technique after submerging the samples in a corrosive solution.

The surface contact resistance of the coating alloy under a 140 N compression force using the four probe technique showed a reading of 15 mΩ cm^2. It was also speculated by Tawfik et al. and Lee et al. [17] that a smoother surface finish may further reduce and/or improve the following bipolar plate characteristics:

- The interfacial resistance.
- The micro potential difference between the MEA and the metallic bipolar plates which may further reduce localized corrosion of the metallic bipolar plates.
- The surface characteristics became hydrophobic which may improve the two-phase flow of the reactant gases and water. Also, Taniguchi and Yasuda [18] stated that gas flow channels of PEMFC were highly water-proofed by plasma polymerization and pretreatment by sandblasting was efficient for increasing water-contact angle of the coated surface. This very low water wetability of gas flow channels particularly where the condensed water inside the fuel cell tends to accumulate, caused noticeable increase in peak power of the fuel cell. Water accumulation or flooding of flow conduits and gas diffusion layer (GDL) will hinder the flow of reactant gases and isolate the catalyst due to submersion resulting in considerable power degradation.

The economic analysis and comparison between graphite composites and carbide-based amorphous metallic coating alloy developed by Tawfik et al. and applied to the Al bipolar plates system showed 22% savings in H_2 consumption. Considering

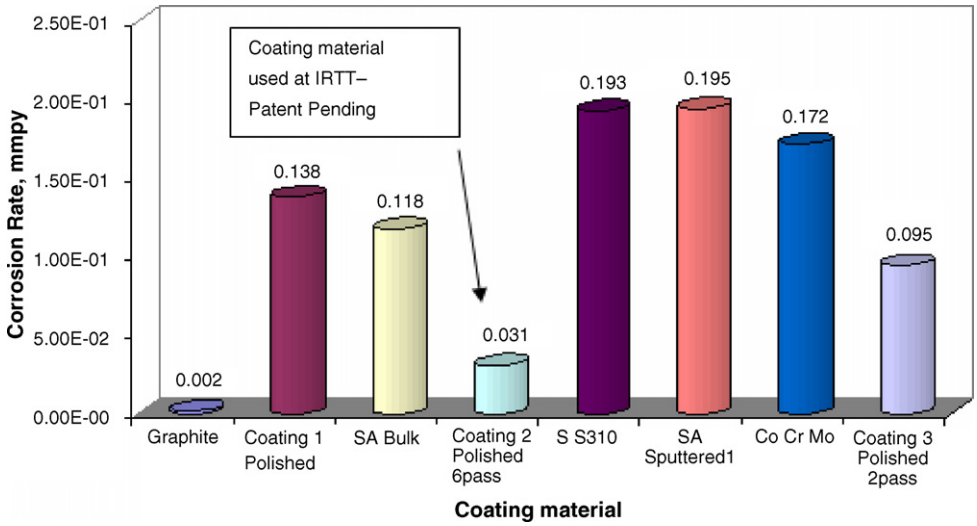

Fig. 3. Corrosion rates for different materials and coatings in 0.5 M Na_2SO_4 + 10 ppm HF solution at 80 °C.

Table 3
Cost analysis

Summary of fixed and running costs	Graphite composite bipolar plates (US$)	Coated aluminum bipolar plates (US$)
Fixed cost of bipolar plates per kiloWatt	130	266
Running cost of hydrogen per kiloWatt hour	0.405	0.372

both running and fixed costs for these two types of plate materials, Table 3 shows a brief comparison and cost analysis of both materials.

The initial cost of metallic bipolar plates is slightly higher due to the secondary manufacturing process. However, after the first 6 months of operation and savings in H_2 consumption, the total cost of graphite composites begins to exceed the metallic plates as depicted in Table 3 and Fig. 4.

Reactant flow field design is one of the most important features of the PEMFC technology. The flow field should be designed to avoid accumulation of condensed water inside the fuel cell on both cathode and anode sides as well as conserve the reactant humidity particularly on the air/oxygen side. Tawfik et al. have tested a number of interdigitated reactant gases flow fields with various levels of flow obstructions ranging from full to partial obstructions to enhance mass transport and heat transfer mechanism from diffusion and natural convection respectively to a more effective forced convection mechanism. Fig. 5 shows that for completely obstructed channels the parasitic energy is predominantly high that could exceed the power generated from the fuel cell. A small obstruction that could reach one-third the total depth of the channel was proven to be the most efficient in this study as shown in Fig. 5.

Natesan and Johnson [19] studied the oxidation and sulfidation of 310 SS and chromium-carbide- and Cr-coated in high O_2 and S environment in a temperature range of 650–875 °C. The use of appropriate corrosion-resistant coatings on metallic components offers an avenue to minimize material degradation and extend their lifetime. The coatings for the test were developed by an electro-spark deposition process in which short duration; high-current electrical pulses were used to deposit the electrode material on the metallic substrate. They observed that

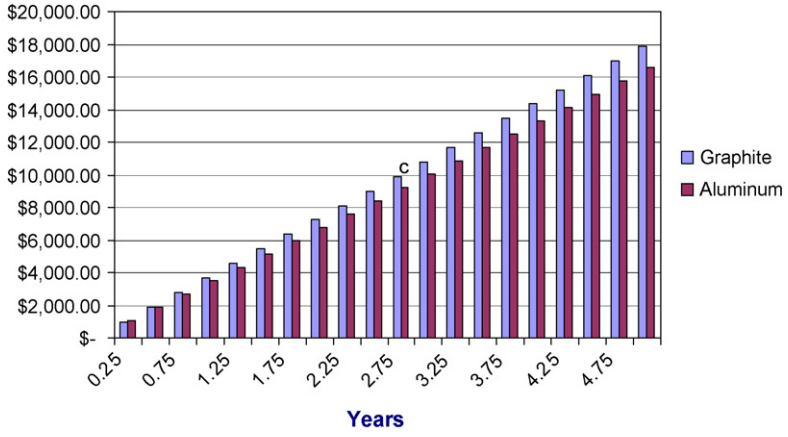

Fig. 4. One kiloWatt fuel cell cost comparison between coated aluminum and graphite bipolar plates.

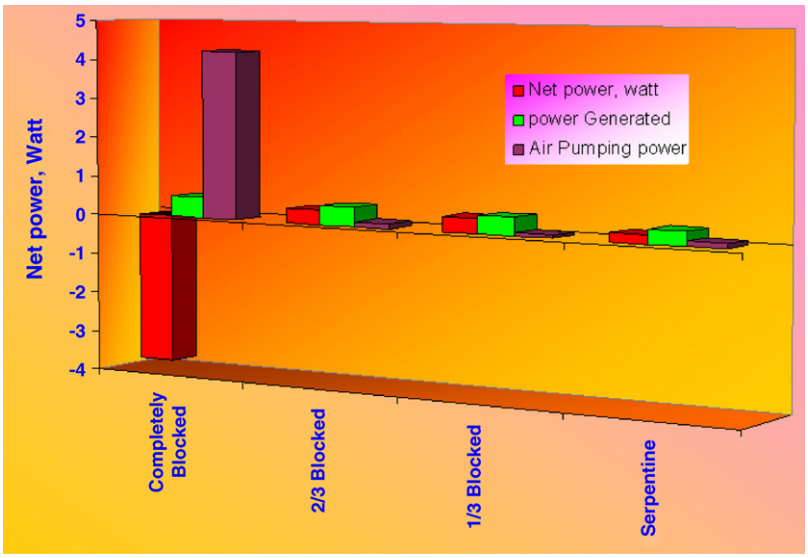

Fig. 5. Interdigitated flow field study.

in a high sulfur environment, the uncoated alloy exhibited severe sulfidation corrosion by means of (Fe, Ni) sulfide formation; the Cr-coated alloy exhibited moderate corrosion whereas the chromium-carbide-coated alloy exhibited the least corrosion. Vickers hardness measurements made by Natesan and Johnson [19] on the surface and as a function of depth showed that the initial high hardness values of chromium-carbide-coated specimens were retained even after oxidation and sulfidation treatment.

2.3.2. Conducting polymer-based coatings

Shine et al. [20] electrochemically coated 304 stainless steel with conducting polymers polyaniline (PANI) and polypyrrole (PPY). Cyclic voltametry was used for the polymerization and deposition of these polymers. The polymer-coated stainless steel plates were tested for corrosion and contact resistance under PEM fuel cell conditions. An improved corrosion resistance with acceptable contact resistance was observed but cost, durability, and volume production were not mentioned in the study.

2.3.3. Fe-based amorphous alloys

Jayaraj et al. [21] investigated the corrosion behavior of two Fe-based amorphous alloys Fe48Cr15Mo14Y2C15B6 and Fe50Cr18Mo8Al2Y2C14B6 under conditions that simulate the fuel cell environment in comparison with those of a stainless steel. H_2 gas and pressurized air were bubbled into a 1 M H_2SO_4C + 2 ppm F^- solution at 75 °C solution, throughout the experiment to simulate the respective anodic and cathodic PEMFC environment. The Fe50Cr18Mo8Al2Y2C14B6 amorphous alloy displayed significantly higher corrosion resistance in relation to the 316SS of identical Cr content. Also, the data indicated that higher Cr content played an important role in improving the corrosion resistance.

2.3.4. Physical vapor deposition (PVD) coating

Lee et al. [22] applied PVD coating of YZU001 like-diamond film on the 5052 Al alloy and 316SS and compared their performance to that of graphite. The corrosion rates were determined by Tafel-extrapolation method from the polarization curves. The coated Al, 316 stainless steel and graphite were fabricated into a single cell to measure contact resistance and to test cell performance. The metallic bipolar plates, PVD-coated 5052 aluminum and 316SS, performed better than the graphite material at the low voltage but experienced shorter cell life. It was also observed that the 316SS plate with its naturally formed passive film had better corrosion rate than the YZU001 coated Al plate. However, the SS contact resistance was higher thus reducing its single cell performance. The Al-coated plates had better contact resistance and single cell performance, however, the cell life was shorter.

2.3.5. Porous materials and metal foams

Kumar and Reddy [23] investigated three different porous materials namely, Ni–Cr metal (Fe: up to 8%, C: up to 2%, Cr: 30–54%, Ni: balance) foam with 50 pores per inch (PPI), 316SS metal foam with 20 PPI, and carbon cloth. The MEA metal ion contamination can be minimized to a great extent by optimizing the fluid-flow in metal foams. In the system, whatever metal ions products are formed; they do not stagnate in the cell stack but are exhausted along with the by-product water [24]. The data were consistent with the metal foams performing better than the conventional channel design flow-field. Furthermore, it was seen that with a decrease in permeability of the metal foam, the cell performance increased. The performance could be further increased by carefully tailoring the size, shape and distribution of pores in the metal foam. An additional advantage will accrue as these metal foams could possibly be used for catalyst support in the electrochemical reactions within the fuel cell, thereby eliminating the need to use carbon electrodes.

2.3.6. Untreated 316SS screens and foils

Wilson et al. [25] focused on development of non-machined and low-cost bipolar plates based on the use of untreated 316SS screens and foils. After building and testing a single cell, they examined the MEA by energy dispersive (EDS) analysis and

found the membrane to be relatively clean. However, EDS cannot quantitatively distinguish metal ions that are present in stainless steel because the scope itself was made of the same material. In order to accurately assess the presence of various metals that might be present in the MEA, the X-ray fluorescence (XRF) spectra were obtained before and after testing the MEA for 2000 h. The final XRF data were consistent with the presence of metals such as Fe and Ni in appreciable quantities.

Many types of alloys have been developed for applications where common stainless steels such as 304 or 316SS do not provide adequate corrosion resistance. In general, the compositions of these alloys are similar to their stainless steel or nickel-base counterparts except that certain stabilizing elements, such as Ni, Cr, and Mo are added or are present in much higher concentrations in order to obtain desirable corrosion properties. However, in neutral to oxidizing media, a high Cr content (which is often accompanied by the addition of Mo) is necessary. These cells were operated at 0.3 MPa (absolute) and at 80 °C. The humidifiers on the anode and cathode sides were heated to 100 and 80 °C, respectively. Purified H_2 was introduced at 0.3 standard liters per minute (SLPM). Compressed room air was provided to the cell at 1.8 SLPM.

Ni levels of 0.85, 0.56, and 2.4 ppm were measured in the anode-face exposed solutions and 0.034, 0.019, and 0.027 ppm Ni in the cathodeface exposed solutions for 0–1500, 1500–3400, and 3400–4100 h segments of exposure, respectively. Cr was not detected and visual analysis of the test coupon showed no evidence of corrosive attack. The Ni–50Cr alloy (no nitridation treatment) had a lower contact resistance than 316 stainless steel, shown for comparative purposes.

X-ray fluorescence (XRF) was used to examine the anode- and cathode-side membranes and ELAT backings from the two, 500 h tests. Only trace levels of Ni and Cr were found, in the range of 0.01–0.3 $\mu g\,cm^{-2}$, which is on the order of the detection limit of this measurement. This very low level of contamination indicates inert and protective behavior by the CrN/Cr_2N surface with few, if any, through thickness pinhole defects. To put this result in context, Wind et al. [2], for example, reported that 316 stainless steel tested for 100 h at 75 °C as a bipolar plate material resulted in Ni contamination levels of 76 $lg\,cm^{-2}$ (see Ref. [2] for specifics of these fuel cell test conditions). It should be noted that some stagnant Cr-rich liquid was found in one of the alignment pin ports on disassembly of the cell. However, no membrane contamination was found in this area. A small Cr–O–C rich surface region ($\sim 0.5 \times 1$ mm) found at this location was likely the source of the Cr-rich liquid. A major casting flaw or inclusion may have led to local poor nitridation, making this area vulnerable to attack, although the stagnant liquid may also have led to more corrosive local conditions against which the Cr-nitride was not sufficiently resistant.

2.4. Composite plates

Composite plates can be categorized as metal- or carbon-based. A metal-based composite bipolar plate has been developed by Los Alamos National Laboratory [26]. This design combines porous graphite, polycarbonate plastic and stainless steel in an effort to leverage the benefits of different materials. Since porous graphite plates production is not as time consuming or expensive as producing non-porous graphite plates, it can be used while impermeability is provided by the stainless steel and polycarbonate parts. Stainless steel also provides rigidity to the structure while the graphite resists corrosion. The polycarbonate provides chemical resistance and can be molded to any shape to provide for gaskets and manifolding. The layered plate appears to be a very good alternative from stability and cost standpoints.

3. Summary and conclusions

Cost and durability are still the two pronounced challenges for the PEM fuel cell industry. The cost of large supplies of fuel cell materials and high volume manufacturing processes must be reduced for PEM to reach an economic viability and allow it to penetrate the energy market and compete with other systems. The durability of the PEM fuel cell is another important parameter that must be improved to enhance the reliability of the two main components, namely bipolar plates and MEA. Further research and development efforts must be conducted to rectify the bipolar plate corrosion mechanisms as described below [11].

3.1. Corrosion failure by pinhole formation

Unfortunately, corrosion processes occur regardless whether the fuel cell is operating or not unless extreme measures are taken to evacuate the fuel cell stack of water. Corrosion failure mode is due to pinhole formation through the bipolar plate, a corrosion rate of about 25 $\mu m\,year^{-1}$ with a corresponding corrosion current density of 2–3 $\mu A\,cm^{-2}$ is acceptable.

3.2. Corrosion failure by electrocatalyst poisoning

Common electrocatalysts include Pt and Pt–Ru alloys that are susceptible to poisoning by adsorption. Most poisoning adsorbents include CO, sulfur, chloride, and low boiling point hydrocarbons. For metallic coatings on Al, little, if any at all, sulfur and chloride will be present eliminating their possible poisoning of catalysts. The same is also true for CO and hydrocarbons if a metallic coating on aluminum is used.

It is possible that O_2 on the cathode side may react with metal ions to form an oxide (e.g., Fe_2O_3, CuO). Since these oxides are not bound to any site, it is probable that they will be flushed from the electrodes by convective action of the air and water on the cathode.

It is possible that the corrosion by-products may react chemically with the oxygen to form an oxide in the electrode. This oxide may or may not leave the electrode causing potential fouling problems within the electrode due to blocked pores.

It may be possible for H_2 gas to reduce the metal ions to their metallic state. The metal deposits would be located in regions where the proton may reside including the liquid phase water and the ionomer coating of the catalysts. In a similar manner to the cathode, the metal deposits may flush out of the electrode via the convective flow action.

Table 4
Summary

Plate material	Coating material (thickness)	Corrosion current density (DOE target 16 μA cm^{-2})/corrosion rate	Contact resistance (DOE target 20 mΩ cm^2),	Cost (DOE2010 target US$ 10 kW^{-1})	Ref.
AISI446, 316SS, 349TM, 2205	Nitrided AISI446	Anode potential CD at −0.1 V at 70 °C, 1 M H_2SO_4 + 2 ppm F^-, with hydrogen purge, AISI446 (−2.0 to −1.0 μA cm^{-2}), 2205 (−0.5–0.5 μA cm^{-2}), 349TM (−4.5 to −2.0 μA cm^{-2}), nitrided AISI1446 (−1.7 to −0.2 μA cm^{-2}), modified AISI446 (−9.0 to −0.2 μA cm^{-2}) Cathode potential CD at 0.6 V at 70 °C, 1 M H_2SO_4 + 2 ppm F^-, with air purge, AISI446 (0.3–1.0 μA cm^{-2}), 2205 (0.3–1.2 μA cm^{-2}), 349TM (0.5–0.8 μA cm^{-2}), nitrided AISI1446 (0.7–1.5 μA cm^{-2}), modified AISI446 (1.5–4.5 μA cm^{-2})	Before operation, AISI446 (190 mΩ cm^2), 2205 (130 mΩ cm^2), 349TM (110 mΩ cm^2), nitrided AISI446 (6 mΩ cm^2), modified AISI446 (4.8 mΩ cm^2), at 140 N cm^{-2}	AISI446 (US$ 4.76 kW^{-1}), 349TM (US$ 4.22 kW^{-1}), 2205 (US$ 3.14 kW^{-1}), nitrided AISI446 (N/A), modified AISI446 (N/A)	[25]
Ni–50Cr alloy, 349TM SS	Thermal nitridation on Ni–50Cr (3–5 μm) and 349TM	Anode environment CD at −0.1 V, at 70 °C, 1 M H_2SO_4 + 2 ppm F^-, with hydrogen purge, nitrided Ni–50Cr (3–4 μA cm^{-2}), nitrided 349TM (15–20 mA cm^{-2}) Cathode environment CD at 0.6 V, with air purge, 349TM (∼0.25 mA cm^{-2})	Before operation, Ni–50CrL (∼60 mΩ cm^2), nitrided Ni–50Cr (∼20 mΩ cm^2), 349 (∼100 mΩ cm^2), nitrided 349 (∼10 mΩ cm^2) at 150 N cm^{-2}		[28]
AISI446	Thermal nitridation on AISI446 (∼1 μm)	Anode environment CD at −0.1 V, at 70 °C, 1 M H_2SO_4 + 2 ppm F^-, with hydrogen purge, nitrided AISI1446 (approximately −1 μA cm^{-2}). Cathode environment CD at 0.6 V, with air purge, nitrided AISI1446 (∼0.6 μA cm^{-2})	Before operation, polarized 7.5 h at 0.6 V, nitrided AISI446 (<40 mΩ cm^2), at 150 N cm^{-2}		[27,29]
AISI434, 436, 441, 444, 446		Anode environment CD at −0.1 V, at 70 °C, 1 M H_2SO_4 + 2 ppm F^-, with hydrogen purge, AISI446 (10–15 μA cm^{-2}), 444 (50 μA cm^{-2}), 436 (60 μA cm^{-2}), 434 (200 μA cm^{-2}), 441 (300 μA cm^{-2}) at 70C, 1 M H_2SO_4 + 2 ppm F^- Cathode environment CD at 0.6 V, with air purge, AISI446 (10–15 μA cm^{-2}), 444 (20 μA cm^{-2}), 436 (20 μA cm^{-2}), 441 (60 μA cm^{-2}), 434 (100 μA cm^{-2}) at 70 °C, 1 M H_2SO_4 + 2 ppm F^-	Before operation AISI446 > 434 > 441 > 436 > 444 (between 100 and 200 mΩ cm^2) at 140 N cm^{-2} (small different) After passivation AISI446 (280 mΩ cm^2 anode environment), (350 mΩ cm^2 cathode environment) at 140 N cm^{-2}		[6,27]
Ni–Cr alloy	Thermal nitridation (3–5 μm)		Before operation, 316 (∼160 mΩ cm^2), Ni–50CrL (∼60 mΩ cm^2), nitrided Ni–50CrL (∼20 mΩ cm^2) at 140 N cm^{-2}		[30]
Ni–Cr alloy, AISI446	Thermal nitridation		Nitrided AISI446 (20 mΩ cm^2), at ∼150 N cm^{-2}		[14]
316SS, Ni–Cr alloy	Thermal nitridation		Before operation, 316 (∼160 mΩ cm^2), Ni–50CrL (∼60 mΩ cm^2), nitrided Ni–50CrL (∼20 mΩ cm^2) at 140 N cm^{-2}, after passivation, nitrided Ni–50CrL (no increase)		[31]

349TM SS, 316, 317L, 904L		Anode environment CD at −0.1 V, at 70 °C, 1 M H_2SO_4 + 2 ppm F^-, with hydrogen purge, 349TM > 904L > 317L > 316 Cathode environment at 0.6 V, with air purge, 349TM > 904L > 317L > 316	Before operation (mΩ cm^2) 316 > 317L > 904L > 349 (160–100 mΩ cm^2) at 140 N cm^{-2} After passivation (mΩ cm^2) 349 (200 mΩ cm^2) at 140 N cm^{-2}		[5]
316SS	Electrochemical process	Electrochemical processed 316 (∼0.030 mmpy), 0.5 M H_2SO_4	Before operation 316 (48 mΩ), electrochemical processed 316 (∼7–27 mΩ) at 15 kgf		[32]
304SS					[33]
316SS	Electrochemical process	0.6 V potential, 0.5 M H_2SO_4, 316 (60 μA cm^{-2}), electrochemical processed 316 (15 μA cm^{-2}), 316SS (0.1 mmpy), electrochemical processed 316 (∼0.030 mmpy)			[17]
316SS, aluminum 5052, graphite	YZU001 on aluminum 5052	Al (1.16 mmpy), Al-coated (0.247 mmpy), 316SS (0.1 mmpy), graphitel (0.019 mmpy), 0.5 M H_2SO_4			[22]
Aluminum, graphite composite	Proprietary coatings (0.1 mm)				[16]
Aluminum, graphite composite	Proprietary coatings (0.1 mm)				[15]
316SS	TiN (2–4 μm)	TiN coating (0.25 μA cm^{-2} with O_2 bubbled solution) and (0.32 μA cm^{-2} with H_2 bubbled solution), 316SS (4.4 μA cm^{-2} with O_2 bubbled solution) and (27.1 μA cm^{-2} with H_2 bubbled solution), at 80 °C, 0.01 M HCI + 0.01 M Na_2SO_4			[12]
316SS		Anode potential CD at −0.11 V, at 80 °C, 0.01 M HCI + 0.01 M Na_2SO_4 bubbled with hydrogen, 316SS (∼1.6 μA cm^{-2})			[34]
Titanium, 316SS, Poco graphite	FC5 (1 μm) on Ti (proprietary)		Before operation 316SS (37 mΩ cm^2), FC5 (∼13 mΩ cm^2), graphite (10 mΩ cm^2) at ∼220 N cm^{-2}		[35]
321SS, 304SS, 347SS, 316SS, Ti, 310SS, 904LSS, Incoloy 800, Inconel 601, Poco graphite			Before operation 321SS (100 mΩ cm^2), 304SS (51 mΩ cm^2), 347SS (53 mΩ cm^2), 316SS (37 mΩ cm^2), Ti (32 mΩ cm^2), 310SS (26 mΩ cm^2), 904SS (24 mΩ cm^2), Incoloy 800 (23 mΩ cm^2), Inconel 601 (15 mΩ cm^2), Poco graphite (10 mΩ cm^2) at 220 N cm^{-2} After 1200 h operation Ti (250 mΩ cm^2), 316SS (44 mΩ cm^2), SS310 (28 mΩ cm^2), Poco graphite (10 mΩ cm^2) at 220 N cm^{-2}		[4]
310SS, 316SS, 904LSS			Before operation 904LSS < 310SS < 316SS; after operation SS310 < 316SS		[36]
Aluminum	Gold-plated aluminum (2 μm)	Aluminum (∼250 μmpy), copper (>500 μmpy), gold-plated aluminum (∼750 μm year^{-1}), 316SS (<100 μmpy), graphite (<15 μmpy), silver (<15 μmpy), gold (<15 μmpy), nickel (>1000 μmpy), phosphorous copper (∼500 μmpy), phosphorous nickel (<30 μmpy), tin (>10000 μmpy), titanium (<100 μmpy), tungsten (<100 μmpy), zinc (>2000 μmpy), 0.5 M H_2SO_4		Graphite (US$ 75 kg^{-1}), conductive plastics (US$ 5–30 kg^{-1}), gold-plated aluminum (US$ 7 kg^{-1})	[9]

Table 4 (*Continued*)

Plate material	Coating material (thickness)	Corrosion current density (DOE target 16 μA cm^{-2})/corrosion rate	Contact resistance (DOE target 20 mΩ cm^2),	Cost (DOE2010 target US$ 10 kW^{-1})	Ref.
Aluminum	Multilayer coating (Ni, Au) conductive polymers (polyaniline)			Graphite (US$ 89 kW^{-1}), gold-plated (US$ 346 kW^{-1}), nickel-plated, (US$ 3.2 kW^{-1}), aluminum (US$ 2.71 kW^{-1})	[11]
316SS, Fe-based alloys—Fe50Cr18Mo8Al2YC14B6		Anode potential CD at −0.1 V at 75 °C, 1 M H_2SO_4 + 2 ppm F^-, with hydrogen bubbling, Fe-based alloy (2.48 μA cm^{-2}) Cathode environment CD at 0.6 V, at 75 °C, 1 M H_2SO_4 + 2 ppm F^-, with air bubbling, Fe-based alloy (0.12 mA cm^{-2})			[21]
316SS, graphite	TiN on 316SS (1 μm)		Before operation 316SS (34.2 mΩ cm^2), 316SS/TiN (32.7 mΩ cm^2), graphite (30.2 mΩ cm^2) at 180 N cm^{-2}		[13]
Titanium, 304SS	Plasma-polymerized HFP				[18]
304SS	NiAl (1 μm)	Corrosion current density, Icorr (49 μA cm^{-2}), 0.5 M H_2SO_4 at 25 °C			[37]
304SS	Conductive polymers polyaniline (PANI) and polypyrrole (PPY)	Corrosion current density, Icorr, 304SS (10 μA cm^{-2}), PPY (1 μA cm^{-2}), PANI (0.1 μA cm^{-2}), 0.1 M H_2SO_4	Before operation 304SS (∼100 mΩ cm^2), PPY (∼800 mΩ cm^2), PANI (∼800 mΩ cm^2), graphite (80 mΩ cm^2) at ∼140 N cm^{-2}		[20]
Ni–Cr metal foam, 316SS metal foam, 316SS channel, carbon cloth					[23]
316SS, titanium	Ti-FC5, 316SSFC6, 316SSFC7		Before operation 316SS (∼40 mΩ cm^2), FC5–7 (∼10–15 mΩ cm^2) at 200 N cm^{-2}		[38]
304LSS, 304LN, 316, 316LN, 317L, 904L, E-brite, SAF2205, SAF2507, AL29-4-2, AL-6XN					[39]
316SS	Gold, proprietary coatings		Oxide resistance −(19.6–668.36 mΩ cm^{-1})		[2]
Aluminum	Graphite overmolded				[40]
SS felt, nickel foam, carbon paper, graphite					[41]
310SS				US$ 6.44 kW^{-1}	[42]
316SS, E-brite, AL600 (nickel-based alloy)		E-brite (<1 μm $year^{-1}$) better than 316SS and AL600			[25]
Aluminum, 316SS, titanium	Gold-plated aluminum and 316SS		Before operation 316SS (∼110 mΩ cm^2), titanium (∼70 mΩ cm^2), graphite (10 mΩ cm^2) at ∼140 N cm^{-2}		[10]
Fe-based alloys			Before operation Fe-based (∼100 mΩ cm^2), Ni-based (∼10 mΩ cm^2), Au-plated (∼2mΩ cm^2) at ∼140 N cm^{-2}		[43]
316SS	Sand-blasted and etched				[44]
310SS, chromium carbide					[19]

3.3. Corrosion failure by membrane ion-exchange

It is possible that the proton groups on the Nafion® side chains may be exchanged with a metal ion from the corroding bipolar plate.

3.4. Corrosion failure by passivation formation

The overall comprehensive testing and evaluation of various materials for metallic and non-metallic bipolar plates are clearly compiled in Table 4 to provide a quick reference of the most up to date research findings in this area of PEM fuel cell technology. The current bipolar plate specifications and the DOE technical and cost targets are described in Table 4.

In summery, the concept of replacing graphite with metallic bipolar plates looks promising. This review gives the reader an update on research that can help attain a balance between metal integrity and power output. As more research gets underway to optimize conditions that are hospitable to metals under the fuel cell operating conditions, an ideal fuel cell system will emerge that can be deployed in the transportation sector.

References

[1] P. Costamagna, S. Srinivasan, J. Power Sources 102 (2001) 253–269.
[2] J. Wind, R. Spah, W. Kaiser, G. Bohm, J. Power Sources 105 (2002) 256–260.
[3] A. Hermann, T. Chaudhuri, P. Spagnol, Int. J. Hydrogen Energy 30 (2005) 1297–1302.
[4] D.P. Davies, P.L. Adcock, M. Turpin, S.J. Rowen, J. Appl. Electrochem. 30 (2000) 101–105.
[5] H. Wang, M.A. Sweikart, J.A. Turner, J. Power Sources 115 (2003) 243–251.
[6] H. Wang, J.A. Turner, J. Power Sources 128 (2004) 193–200.
[7] V. Mehta, J.S. Cooper, J. Power Sources 144 (2003) 32–53.
[8] R.L. Borup, N.E. Vanderborgh, Mater. Res. Soc. Symp. Proc. 393 (1995) 151–155.
[9] A.S. Woodman, E.B. Anderson, K.D. Jayne, M.C. Kimble, American Electroplaters and Surface Finishers Society 1999, AESF SUR/FIN'99 Proceedings, June 21–24, 1999.
[10] P.L. Hentall, J.B. Lakeman, G.O. Mepsted, P.L. Adcock, J.M. Moore, J. Power Sources 80 (1999) 235–241.
[11] M.C. Kimble, A.S. Woodman, E.B. Anderson, American Electroplaters and Surface Finishers Society 1999, AESF SUR/FIN'99 Proceedings, June 21–24, 1999.
[12] M. Li, S. Luo, C. Zeng, J. Shen, H. Lin, C. Cao, Corros. Sci. 46 (2004) 1369–1380.
[13] E.A. Cho, U.-S. Jeon, S.-A. Hong, I.-H. Oh, S.-G. Kang, J. Power Sources 142 (2005) 177–183.
[14] M.P. Brady, P.F. Tortorelli, K.L. More, H.M. Meyer III, L.R. Walker, H. Wang, J.A. Turner, B. Yang, R.A. Buchanan, Cost-effective surface modification for metallic bipolar plates, DOE FY 2004 Progress Report.
[15] Y. Hung, K. El-Khatib, H. Tawfik, ASME—The 2nd International Conference on Fuel Cell Science, Engineering and Technology, RIT, Rochester, New York, June 14–16, 2004.
[16] Y. Hung, H. Tawfik, ASME—The 3rd International Conference on Fuel Cell Science, Engineering and Technology, Ypsilanti Marriott Hotel at Eagle Crest, Ypsilanti, MI, May 23–25, 2005.
[17] S.J. Lee, C.H. Huang, J.J. Lai, Y.P. Chen, J. Power Sources 131 (2004) 162–168.
[18] A. Taniguchi, K. Yasuda, J. Power Sources 141 (2005) 8–12.
[19] K. Natesan, R.N. Johnson, Surf. Coat. Technol. 33 (1987) 341–351.
[20] J. Shine, J.C. McClure, R. Chianelli, P. Pich, P.J. Sebastian, Int. J. Hydrogen Energy 30 (2005) 1339–1344.
[21] J. Jayaraj, Y.C. Kim, K.B. Kim, H.K. Seok, E. Fleury, Sci. Technol. Adv. Mater. 6 (2005) 282–289.
[22] S.J. Lee, C.H. Huang, Y.P. Chen, J. Mater. Process. Technol. 140 (2003) 688–693.
[23] A. Kumar, R.G. Reddy, J. Power Sources 129 (2004) 62–67.
[24] A. Kumar, R.G. Reddy, PEM Fuel Cell Bipolar Plate Material Selection Design and Integration, TMS, Seatlle, WA, February 2002, pp. 41–53.
[25] M.S. Wilson, C. Zawodzinski, S. Møller-Holst, D.N. Busick, F.A. Uribe, T.A. Zawodzinski, Proceedings of the 1999 U.S. DOE Hydrogen Program Review, 1999.
[26] Los Alamos National Laboratory Home Page, 1998 (available from World Wide Web: http://www.ott.doe.gov/pdfs/contractor; last retrieved 5 November 2001).
[27] J.A. Turner, H. Wang, M.P. Brady, Corrosion Protection of Metallic Bipolar Plates for Fuel Cells, May 22–26, DOE Hydrogen Program Review, 2005, available online at http://www.nrel.gov/docs/fy05osti/38190.pdf.
[28] H. Wang, M.P. Brady, G. Teeter, J.A. Turner, J. Power Sources 138 (2004) 86–93.
[29] H. Wang, M.P. Brady, K.L. More, H.M. Meyer III, J.A. Turner, J. Power Sources 138 (2004) 79–85.
[30] M.P. Brady, K. Weisbrod, I. Paulauskas, R.A. Buchanan, K.L. More, H. Wang, M. Wilson, F. Garzon, L.R. Walker, Scripta Mater. 50 (2004) 1017–1022.
[31] M.P. Brady, K.L. More, P.F. Tortorelli, L.R. Walke, K. Weisbrod, M. Wilson, F. Garzon, H. Wang, I. Paulauskas, R.A. Buchanan, Cost-effective surface modification for metallic bipolar plates, DOE FY 2003 Progress Report.
[32] S.J. Lee, J.J. Lai, C.H. Huang, J. Power Sources 145 (2005) 362–368.
[33] S.J. Lee, Y.P. Chen, C.H. Huang, J. Power Sources 145 (2005) 369–375.
[34] M.C. Li, C.L. Zeng, S.Z. Luo, J.N. Shen, H.C. Lin, C.N. Cao, Electrochim. Acta 48 (2003) 1735–1741.
[35] D.R. Hodgson, B. May, P.L. Adcock, D.P. Davies, J. Power Sources 96 (2001) 233–235.
[36] D.P. Davies, P.L. Adcock, M. Turpin, S.J. Rowen, J. Power Sources 86 (2000) 237–242.
[37] S.K. Chen, H.C. Lin, C.Y. Chung, Corrosion resistance study of stainless-steel bipolar plates with NiAl coatings, Feng Chia University and National Science Council of Republic of China Under the Grant Numbers FCU-93GB27 and NSC 93-2218-E-35-006.
[38] G.M. Griffths, E.E. Farndon, D.R. Hodgson, I.M. Long, The Knowledge Foundation's 3rd Annual International Symposium, Washington, D.C., April 22–24, 2001.
[39] J.S. Kim, W.H.A. Peelen, K. Hemmes, R.C. Makkus, Corros. Sci. 44 (2002) 635–655.
[40] S. Ehrenberg, D. Baars, J. Kelly, I. Kaye, One Piece Bi-polar Plate with Cold Plate Cooling, Dais Analytic Corporation/Rogers Corporation, 2002.
[41] S. Gamburzev, A.J. Appleby, J. Power Sources 107 (2002) 5–12.
[42] F.J. Chimbole, J.P. Allen, R.M. Bernard, Results of PEMFC bipolar separator plate interconnect and current collector development at AEC (www.gencellcorp.com).
[43] R. Hornung, G. Kappelt, J. Power Sources 72 (1998) 20–21.
[44] C.E. Reid, W.R. Mérida, G. McLean, Proceedings of 1998 Fuel Cell Seminar, Palm Spring, 1998.
[45] I. Zafar, J. Guiheen, N. Dave, R. Timothy, World Patent WO00,128,019 (19 April 2001).
[46] T. Matsumoto, J. Niikura, H. Ohara, M. Uchida, H. Gyoten, K. Hatoh, E. Yasumoto, T. Kanbara, K. Nishida, Y. Sugawara, Europeon Patent EP1,094,535 (25 April 2001).
[47] Y. Li, W. Meng, S. Swathirajan, S. Harris, G. Doll, US Patent 5,624,769 (20 April 1997).